

Short Gamma-Ray Bursts and Gravitational-Wave Observations from Eccentric Compact Binaries

Wei-Wei Tan^{1,2,3}, Xi-Long Fan¹ & F. Y. Wang^{2,3*}

¹Hubei University of Education, 430205, Wuhan, Hubei, China

²School of Astronomy and Space Science, Nanjing University, Nanjing 210093, China

³Key Laboratory of Modern Astronomy and Astrophysics (Nanjing University), Ministry of Education, Nanjing 210093, China

ABSTRACT

Mergers of compact binaries, such as binary neutron stars (BNSs), neutron star-black hole binaries (NSBHs), and binary black holes (BBHs), are expected to be the best candidates for the sources of gravitational waves (GWs) and the leading theoretical models for short gamma-ray bursts (SGRBs). Based on the observations of SGRBs, we could derive the merger rates of these compact binaries, and study the stochastic GW backgrounds (SGWBs) or the co-detection rates of GWs associate with SGRBs (GW-SGRBs). But before that, the most important thing is to derive the GW spectrum from a single GW source. Usually, GW spectrum from a circular orbit binary is assumed. However, observations of the large spatial offsets of SGRBs from their host galaxies imply that SGRB progenitors may be formed by the dynamical processes, and will merge with residual eccentricities (e_r). The orbital eccentricity has important effect on GW spectra, and therefore on the SGWB and GW-SGRB co-detection rate. Our results show that the power spectra of the SGWBs from eccentric compact binaries are greatly suppressed at low frequencies (e.g., $f \lesssim 1$ Hz). Especially, SGWBs from binaries with high residual eccentricities (e.g., $e_r \gtrsim 0.1$ for BNSs) will hard to be detected (above the detection frequency of ~ 100 Hz). For the co-detection rates of GW-SGRB events, they could be ~ 1.4 times higher than the circular case within some particular ranges of e_r (e.g., $0.01 \lesssim e_r \lesssim 0.1$ for BBH), but greatly reduced for high residual eccentricities (e.g., $e_r > 0.1$ for BNSs). In general, the BBH progenitors produce 200 and 10 times higher GW-SGRB events than the BNS and NSBH progenitors, respectively. Therefore, binaries with low residual eccentricities (e.g., $0.001 \lesssim e_r \lesssim 0.1$) and high total masses will easier to be detected by aLIGO. However, only a small fraction of BBHs could be SGRB progenitors (if they can produce SGRBs), because the predicted GW-SGRB event rate (60–100 per year) is too high compared with the recent observations, unless they merge with high residual eccentricities (e.g., $e_r > 0.7$).

Key words: gamma rays: bursts - gravitational waves - stars: late type

1 INTRODUCTION

Binary compact objects, such as binary neutron stars (BNSs), neutron star-black hole binaries (NSBHs), and binary black holes (BBHs) are expected to be the best candidates for the sources of gravitational waves (GWs; e.g., Abbott et al. 2016c,d), which are expected to be detected by LIGO (e.g., Abbott et al. 2008, 2009; Aasi et al. 2015) and Virgo (e.g., Acernese et al. 2008, 2015). Theoretically, short GRBs (SGRBs), with duration time $T_{90} < 2$ s (Kouveliotou et al. 1993), are believed to originate from the mergers of BNSs or NSBH binaries (Paczynski 1986; Eichler et al. 1989; Paczynski 1991; Meszaros & Rees 1992; Narayan, Paczynski, & Piran 1992). Observations of SGRBs, such

as the non-detection of supernova associations, large offsets of their locations in the host galaxies, and a possible kilonova association (e.g., GRB 130603B; Tanvir et al. 2013), support the hypothesis of the coalescing model (Berger 2014). Except for the electromagnetic radiation (EMR), the coalescences of compact binaries could generate strong GWs in the sensitive frequency band of the ground-based GW detectors (Thorne 1987). On August 17 2017, the Advanced LIGO (aLIGO) and Advanced Virgo (aVirgo) discovered the GW170817 from a binary neutron star inspiral (Abbott et al. 2017b), and the associated GRB 170817A was observed 1.7 s after the coalescence time (von Kienlin et al. 2017; Connaughton et al. 2017; Goldstein et al. 2017a,b; Savchenko et al. 2017b,c; Abbott et al. 2017c). This observation directly proved the coalescing model for SGRBs. It is quite expected that more observations of GWs associated with

* E-mail: fayinwang@nju.edu.cn

SGRBs (GW-SGRB) will uncover the nature of SGRB central engine (Aasi et al. 2014; Regimbau et al. 2015).

Except for BNSs and NSBHs, recent observations show that BBHs may also be SGRB progenitors (e.g., Connaughton et al. 2017; Verrecchia et al. 2017). On September 14, 2015, aLIGO detected the first transient GW event called GW150914 (Abbott et al. 2016a), which was produced by the final in-spiral and ring-down phases of a BBH system with component masses of $m_1 = 36.2^{+5.2}_{-3.8} M_\odot$ and $m_2 = 29.1^{+3.7}_{-2.3} M_\odot$ (Abbott et al. 2016c). The *Fermi* gamma-ray burst monitor (GBM) observed a weak transient source above 50 keV, 0.4 s after the GW event, which could be a possible weak SGRB (Connaughton et al. 2016; Savchenko et al. 2016). The second GW event, GW151226, was observed by the twin detectors of aLIGO on December 26, 2015 (Abbott et al. 2016b). The inferred initial BH masses are $14.2^{+8.3}_{-3.7} M_\odot$ and $7.5^{+2.3}_{-2.3} M_\odot$, and the final BH mass is $20.8^{+6.1}_{-1.7} M_\odot$. However, no EMR was observed by the following observations (Adriani et al. 2016; Cowperthwaite et al. 2016). The third GW event, GW170104, was observed by the twin advanced detectors of LIGO on January 4, 2017 (Abbott et al. 2017a). The inferred black hole masses are $31.2^{+8.4}_{-6.0} M_\odot$ and $19.4^{+5.3}_{-5.9} M_\odot$, and the final black hole mass is $48.7^{+5.7}_{-4.6} M_\odot$. The *Fermi* Gamma-ray Burst Monitor (GBM) and Large Area Telescope (LAT) observations found no electromagnetic counterparts for GW170104 (*Fermi*-GBM & *Fermi*-LAT collaborations 2017). Interestingly, the data from the Mini-Calorimeter (MCAL) on board AGILE satellite shows a weak EMR event before GW170104 (E2), and the significance for a temporal coincidence is 3.4σ (Verrecchia et al. 2017). However, observation from the International Gamma-Ray Astrophysics Laboratory (INTEGRAL) challenges their result (Savchenko et al. 2017a). The fourth GW event of GW170814 was observed by a three-detector network, and the inferred masses of BHs are $30.5^{+5.7}_{-3.0} M_\odot$ and $25.3^{+2.8}_{-4.2} M_\odot$ (Abbott et al. 2017d). Still, no obvious optical counterparts were detected (e.g., Arcavi et al. 2017). For the fifth GW event of GW170608, the inferred BH masses are $12^{+7}_{-2} M_\odot$ and $7^{+2}_{-2} M_\odot$ (Abbott et al. 2017e), and no EMR counterparts were reported. If BBHs are confirmed to be the progenitors of SGRBs, then SGRB model will need to be modified (e.g., Loeb 2016; Zhang 2016), because generally mergers of BBHs can not produce GRBs.

The coalescence processes of compact binaries could be divided into three phases: in-spiral, merger and ring-down (e.g., Flanagan & Hughes 1998; Bartos, Brady, & Márka 2013). For the in-spiral phase, the emitted GW frequencies are in the most sensitive band of LIGO/Virgo and are of the most interest, which have been investigated by numerous authors with circular orbit (e.g., Tumlinson & Shull 2000; Regimbau & Mandic 2008; Rosado 2011; Clark et al. 2015). BNSs in our Milky Way Galaxy, whose progenitors are the massive binary stars¹, always have low-kick velocities ($\lesssim 50 \text{ km s}^{-1}$; Bhattacharya & van den Heuvel 1991; Portegies Zwart & Yungelson 1998; Dewi, Podsiadlowski, & Pols 2005), and their orbits are nearly circular before the GWs enter the detection band of LIGO/Virgo (e.g., binary pulsar PSR 1913 + 16 is expected to enter the detection frequency of 15 Hz with the residual eccentricity of 10^{-6} ; Peters & Mathews 1963; Kalogera et al. 2001; Osłowski et al. 2011). However, some SGRBs detected in or near the elliptical galaxies always

have large spatial offsets, which cannot be attributed by the kick velocity. For example, GRB 050509b with an offset of $40 \pm 13 \text{ kpc}$ implies a kick velocity of $200 \text{ km s}^{-1} \lesssim v \lesssim 600 \text{ km s}^{-1}$ (e.g., Grindlay et al. 2006). This is inconsistent with the Hulse-Taylor binary pulsar (Hulse & Taylor 1975) or the BNSs known in our Galaxy that were formed by the evolution of massive binary systems (Bhattacharya & van den Heuvel 1991; Portegies Zwart & Yungelson 1998). These are all probably low-kick velocity ($\lesssim 50 \text{ km s}^{-1}$) systems and thus are expected to remain within the central potential of their parent galaxies (Dewi, Podsiadlowski, & Pols 2005). Additionally, the birth kicks of black holes in low-mass X-ray binaries (LMXB) also do not require to exceed 100 km/s (Mandel 2016). Numerical simulations show that this kind of SGRBs could be originated from the mergers of BNSs formed by dynamical captures in core-collapsed globular clusters (Grindlay et al. 2006). In these globular clusters, *n*-body interactions may result in the mergers of binaries with sizable eccentricities (e.g., Anderson et al. 1990). Nearly 10%~30% of SGRBs may formed by this mechanism (Grindlay et al. 2006). One possible evidence for binary formed by dynamical processes is the millisecond pulsar M15-C, whose companion is a neutron star (Anderson et al. 1990). The formation mechanism could be a NS exchange interaction with a cluster LMXB, leading to the production of a NS-NS binary with an orbital eccentricity of $e = 0.68$. Observations of millisecond pulsar PSR J1903+0327 with a main-sequence star companion in a high eccentric orbit ($e = 0.44$) may also support the dynamical capture mechanism (Champion et al. 2008). Observations of LMXBs or X-ray sources by *Chandra* and *XMM-Newton* suggest that the stellar encounters are common in globular clusters (Gendre, Barret, & Webb 2003; Heinke et al. 2003; Pooley et al. 2003). The dynamically captured NSBHs would also allow mergers with high eccentricities. The merger rate in globular clusters peaks at $8 - 25 \text{ yr}^{-1} \text{ Gpc}^{-3}$ for fiducial systems (Lee et al. 2010) and $30 - 100 \text{ yr}^{-1} \text{ Gpc}^{-3}$ for linearly extrapolation (Stephens et al. 2011). Therefore, mergers of eccentric NSBHs could also contribute significantly to SGRB population. O’Leary et al. (2009) found that the the merger rate of the eccentric BBHs in galactic nuclei detectable by LIGO is $\sim 1 - 10^2 \text{ yr}^{-1}$, and the actual merger rate is likely ~ 10 times higher. If BBHs could be SGRB progenitors, a significant fraction of SGRBs could be contributed by the mergers of eccentric BBHs. Numerical simulations show that these dynamically captured systems will merge with a sizable eccentricity and enter the observation frequency window of LIGO/Virgo (East & Pretorius 2012; East et al. 2013; Gold et al. 2012; Samsing et al. 2014). Another mechanism that could lead to high-eccentric-binary merger within Hubble time is the the Kozai oscillation in the triple system in galactic nuclei (Thompson 2011; Antonini & Perets 2012), which could contribute nearly 10% of the coalesce rate to SGRBs (Abadie et al. 2010a).

Given that a large fraction of SGRB progenitors could be the eccentric compact binaries, and the effects of the eccentricity on GW signal search are non-negligible (e.g., $e \gtrsim 0.02$; Brown & Zimmerman 2010; Huerta & Brown 2013; Coughlin et al. 2015), we will study the effects of the eccentricity on both the SGWB and GW-SGRB co-detection rate. In fact, SGWBs from the eccentric orbit binaries have been studied by many previous works, such as SGWBs from the eccentric BNSs in our Galaxy (Ignatiev et al. 2001), SGWBs from the eccentric supermassive BBHs (Enoki & Nagashima 2007), SGWBs from the eccentric Population III binaries (Kowalska et al. 2012), and SGWBs from the long-lived eccentric BNSs (Evangelista & de Araujo 2015). In this paper, three types of SGRB progenitors (including

¹ Usually, the component masses of the massive binaries are assumed within $8 \sim 40 M_\odot$ (e.g., Bhattacharya & van den Heuvel 1991; Portegies Zwart & Yungelson 1998)

BNSs, NSBHs, and BBHs) are considered as the GW sources. SGWBs are generated by these progenitors including triggered and untriggered SGRBs. For the co-detection rate of GW-SGRBs, only GW events with signal to noise ratio (SNR) higher than 8 that triggered the GRB detector are considered. While calculating the SNR, we only considered the in-spiral phase for low mass systems (like BNS or NSBH), because GW frequencies from the merger and ring-down phases are higher than the sensitive frequency band of aLIGO/aVirgo. But for high mass systems (like BBHs), three phases are all considered. Only the gamma-ray radiation happen to point at earth could be observed as GRBs. Therefore, just a small fraction of GW events associate with SGRBs could be observed, because the opening angles of SGRBs are always small (Fong et al. 2014). However, there are many advantages for GW-SGRB observations, e.g., improving the detection probability of GW signal in comparison with an arbitrary stretch of data (Williamson et al. 2014; Bartos & Marka 2015; Clark et al. 2015). Therefore, GWs associate with SGRBs will be an optimal direction for the detection of GW signals. In our calculation, all SGRBs are assumed to originate from the mergers of eccentric compact binaries. It is perhaps even more likely that not all SGRBs are generated from the eccentric compact binaries. We thus expect that our predictions for the event rates are optimistic.

2 SGRB RATE

In this section, we will constrain the SGRB burst rate. Following Tan & Wang (2015) (where long GRBs are considered), we will fit the observed SGRB peak photon flux distribution (PPFD; in unit of photons/s/cm²) and redshift distribution (RD) simultaneously to derive the luminosity function (LF) and the SGRB rate. The peak photon flux (PPF) and redshift data are taken from the *Swift* archive². We also include some probable SGRBs mentioned in literature (Dietz 2011; Kopač et al. 2012; Berger 2014). Finally, we obtained 87 SGRBs with PPFs (in the energy band of 15-150 keV) and 38 SGRBs with redshifts. The PPFD and RD are shown in the bottom panel of Figure 1 by red circles and blue diamonds, respectively. The error bars along y-axis are the statistical errors (i.e., square root of the number in each bin $\Delta N = \sqrt{N}$), which correspond to 68% Poisson confidence intervals for the binned events. The error bars of x-axis represent the bin size.

In order to derive the SGRB burst rate, we firstly introduce the parameters as follows. $\Phi_p(L)$ is the LF with $L_{\min} = 10^{49}$ erg s⁻¹ and $L_{\max} = 10^{55}$ erg s⁻¹ for normalization. $\eta(P_E)$ is the flux triggering efficiency of *Swift* (Lien et al. 2014),

$$\eta(P_E) = \frac{a(b + cP_E/P_{E,0})}{(1 + P_E/dP_{E,0})} \quad (1)$$

for $P_E > 5.5 \times 10^{-9}$ erg s⁻¹ cm⁻², and below this range the function equals to zero (which is suggested to be better than a single detection threshold (Howell et al. 2014; Tan & Wang 2015)). The parameters are as follows: $a=0.47$, $b=-0.05$, $c=1.46$, $d=1.45$ and $P_{E,0} = 1.6 \times 10^{-7}$ erg s⁻¹ cm⁻² (Howell et al. 2014).

P_E is the peak energy flux in units of erg/s/cm², which could be related to the peak photon flux (P) by

$$P_E(P, z) = \frac{P}{(1+z)} \frac{\int_{15(1+z)}^{150(1+z)} ES(E)dE}{\int_{15(1+z)}^{150(1+z)} S(E)dE} \text{ keV}, \quad (2)$$

where $S(E)$ is the prompt spectrum of SGRB, which is well modeled by the band function (Band et al. 1993). The spectral indices are -0.5 and -2.3 below and above the peak energy, respectively. The peak energy could be derived by the $E_p - L_p$ relation proposed by Tsutsui et al. (2013),

$$L_p = 10^{52.29 \pm 0.066} \text{ erg s}^{-1} \left[\frac{E_p(1+z)}{774.5 \text{ keV}} \right]^{1.59 \pm 0.11}, \quad (3)$$

with the linear correlation coefficient is 0.98 and the chance probability is 1.5×10^{-5} (Tsutsui et al. 2013). Zhang & Wang (2017) found a similar correlation using more SGRBs (Zhang & Wang 2017).

The peak photon flux in the detector can be transformed into the peak luminosity in a straightforward way if the redshift is known. We describe it as

$$L_p = 4\pi d_L(z)^2 P_E(P) \mathcal{K}(z). \quad (4)$$

Here $\mathcal{K}(z)$ is the correction factor, which is to convert the observed energy band of 15 – 150 keV to the rest frame band of 1 – 10⁴ keV. We describe it by

$$\mathcal{K}(z) = \frac{\int_{15(1+z)}^{150(1+z)} ES(E)dE}{\int_1^{10^4} ES(E)dE}. \quad (5)$$

For the luminosity function, a broken power-law form is assumed, which is given by

$$\Phi_p(L) \propto \begin{cases} \left(\frac{L}{L_b}\right)^{-\alpha}, & L \leq L_b, \\ \left(\frac{L}{L_b}\right)^{-\beta}, & L > L_b, \end{cases}, \quad (6)$$

where L is the peak luminosity in the energy band of 1 – 10⁴ keV, and α and β are the power law indices below and above the break luminosity L_b . If α equals to β , the LF transforms into a single power law form.

$R_{\text{SGRB}}(z)$ is the observed SGRB rate, which could be related to the star formation rate (SFR) by

$$R_{\text{SGRB}}(t) \propto \int R_{\text{SFR}}(t - \tau) P_\tau(\tau) d\tau, \quad (7)$$

where $R_{\text{SFR}}(t)$ is the SFR and t is the cosmic time corresponding to redshift z . τ is the time delay between the star formation and the occurrence of SGRB, and $P_\tau(\tau)$ is the probability distribution function of τ .

For the parameters defined above, the expected number of SGRBs with observed PPF between P_1 and P_2 that triggered BAT onboard *Swift* can be expressed by

$$N(P_1, P_2) = \frac{\Delta\Omega}{4\pi} T \int_0^\infty \int_{L_{\min}}^{L_{\max}} \eta(P_E) \Phi_p(L) R_{\text{SGRB}}(z) dL \frac{dV(z)}{1+z}, \quad (8)$$

with $P_E = P_E(P, z)$, $L = L(z, P_E)$. The expected number of SGRBs within redshift range of $z_1 < z < z_2$ is given by

$$N(z_1, z_2) = \frac{\Delta\Omega}{4\pi} T \int_{z_1}^{z_2} \int_{L_{\min}}^{L_{\max}} \eta(P_E) \Phi_p(L) R_{\text{SGRB}}(z) dL \frac{dV(z)}{1+z}, \quad (9)$$

where $(\Delta\Omega/4\pi) \sim 0.1$ is the field view of BAT, $T \sim 10$ yrs is the observation time period, $\eta(P_E)$ is the triggering function, $dV(z)$ is the comoving volume element, $1/(1+z)$ accounts for the time dilation.

There is an agreement that SGRB rates do not trace the SFRs directly but with a time delay. Usually, a power-law time delay distribution ($P_\tau \propto \tau^{-1}$) and a lognormal time delay distribution are considered. However, it is found that a power-law

² http://swift.gsfc.nasa.gov/docs/swift/archive/grb_table.

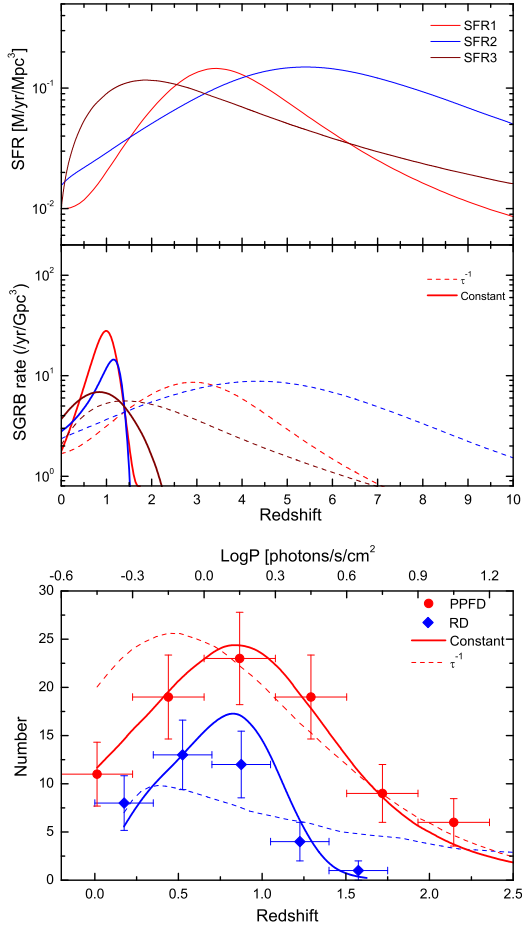


Figure 1. Top: Cosmic star formation rates used in this paper. SFR from Robertson & Ellis (2012) and Wang (2013) (SFR1; red line), SFR from Springel & Hernquist (2003) (SFR2; blue line), and SFR from Fardal et al. (2007) (SFR3; wine line). Middle: The corresponding SGRB rates with a power law time delay distribution ($P_\tau \propto \tau^{-1}$; dashed lines) and a constant time delay distribution (solid lines), respectively. Bottom: The best-fitting results of the peak photon flux distribution (PPFD; top label) and the redshift distribution (RD; bottom label) for SFR1.

time delay distribution is disfavored but a lognormal time delay distribution with $\tau \gtrsim 3$ Gyr is consistent with the observations (Ando 2004; Guetta & Piran 2006; Guetta et al. 2009; Hao & Yuan 2013; Wanderman & Piran 2015). For the lognormal distribution, Wanderman & Piran (2015) found that the width of the distribution is $\sigma \lesssim 0.2$ at 68% confidence level, which corresponds to a very small spread by a factor of $\lesssim 1.2$ in the time delays. Therefore, a constant time delay distribution is assumed in our work for simple, which can be expressed by $R_{\text{SGRB}}(t) \propto R_{\text{SFR}}(t - \tau)$. Here, we consider three SFR models: SFR derived from long GRBs (SFR1; red line; Robertson & Ellis 2012; Wang 2013), SFR derived from cosmological smoothed particle hydrodynamics numerical simulations (SFR2; blue line; Springel & Hernquist 2003), and SFR derived from observations (SFR3; wine line; Fardal et al. 2007), which are shown in the top panel of figure 1.

The free parameters of α , β , L_b , and τ are fitted jointly with PPFD and RD. Firstly, we give an arbitrary set of values for the free parameters. Then, for each set of the parameters, we calculate the χ^2 values (Pearson's chi-squared value) for both PPFD and

Table 1. The best-fitting results for different SFR models with the constant time delay distribution of P_τ .

Model	$R_{\text{SGRB}}(0) (\text{yr}^{-1} \text{Gpc}^{-3})$	τ (Gyr)	$\alpha = \beta$	χ^2	Q
SFR1	$1.77^{+0.4}_{-0.31}$	$3.65^{+0.28}_{-0.39}$	$1.6^{+0.06}_{-0.06}$	6.18	0.52
SFR2	$2.8^{+0.62}_{-0.46}$	$3.88^{+0.18}_{-0.45}$	$1.6^{+0.05}_{-0.05}$	5.89	0.55
SFR3	$3.7^{+0.85}_{-0.61}$	$2.52^{+0.98}_{-1.3}$	$1.6^{+0.05}_{-0.05}$	2.38	0.94

Notes: The best-fitting parameters for three SFR models. $R_{\text{SGRB}}(0)$ is the observed local SGRB rate, τ is the constant time delay between SFR and SGRB rate, α and β are the power law indices of the LF in equation (6), χ^2 is the global chi-squared value, and Q represents the probability to find a new total χ^2 exceeding the current one.

RD. The total χ^2 is assumed to be the linear combination of χ^2_{PPFD} and χ^2_{RD} . The best-fitting parameters are derived by minimizing the global χ^2 . Finally, we show the best-fitting parameters with 1σ errors and Q values (the probability to find a new total χ^2 exceeding the current one) for different SFR models in Table 1. The corresponding SGRB rates are shown in the middle panel of figure 1. For comparison, we fitted the PPFD and RD for SFR1 with a constant time delay distribution and a power law time delay distribution ($P_\tau \propto \tau^{-1}$), simultaneously. The best fitting results are shown in the bottom panel of figure 1. It is obvious that the constant time delay distribution (thick lines) fits the observations quite well, while the power-law time delay distribution (thin lines) fits quite bad, because it produces too many dim SGRBs at high redshifts. The same situation occurs in the other two SFR models.

Given that SGRBs are originated from the mergers of compact binaries, we could be able to predict the total merger rate of their progenitors, where the beaming effect should be considered. Observations of jet breaks in SGRB afterglows can be used to constrain the jet opening angles (Sari et al. 1999). Some SGRBs with jet break observed have been used to derive the opening angles, e.g., GRB 051221A (7°), GRB090426 ($5^\circ - 7^\circ$), GRB11020A ($3^\circ - 8^\circ$), GRB 130603B ($4^\circ - 8^\circ$) (please refer to Fong et al. (2014) for review). However, there are many SGRBs without jet break observation in their afterglows, and only the lower limits of the opening angles could be given, e.g., GRB 050709 with $\theta_j > 15^\circ$. Therefore, we use $\theta_j = 5^\circ$ and $\theta_j = 20^\circ$ as the lower and upper limits for the opening angle to infer the total binary merger rate

$$R_{\text{merger}} \propto R_{\text{SGRB}} / (1 - \cos \theta_j), \quad (10)$$

where we assume that all SGRBs are produced by the mergers of compact binaries.

3 SGWB FROM ECCENTRIC ORBIT BINARIES

SGWBs from the circular orbit binaries have been well studied (Tumlinson & Shull 2000; Regimbau & Mandic 2008; Rosado 2011; Wu et al. 2012; Zhu et al. 2013; Clark et al. 2015). Considering the progenitors of SGRBs could be eccentric compact binaries, we will study the effects of eccentricity on SGWB in this section (Ignatiev et al. 2001; Enoki & Nagashima 2007; Kowalska et al. 2012; Evangelista & de Araujo 2015), and compare it with the ground-based detectors (Kowalska et al. 2012).

Different from the circular orbit binaries, the velocity on the eccentric orbit changes over its period, and the instantaneous orbital frequency also varies. Therefore, binaries will radiate GWs across some range of frequencies but not at one particular frequency. For

the in-spiral phase, the instantaneous spectrum of GWs emitted by the eccentric orbit binaries in the source rest frame can be describe by (e.g., Peters & Mathews 1963; Kowalska et al. 2012)

$$\frac{dE_i}{df_{gw}^n} = \frac{\pi}{3} \frac{1}{G} \left(\frac{4}{n^2} \right)^{1/3} \frac{(GM_{\text{chirp}})^{5/3}}{(f_{gw}^n \pi)^{1/3}} \frac{g(n, e)}{\Psi(e)}, \quad (11)$$

and the spectrum at a special frequency could be described by

$$\frac{dE_i}{df_{gw}} = \sum_{n=2}^{\infty} \delta(f_{gw} - f_{gw}^n) \left. \frac{dE_i}{df_{gw}^n} \right|_{f_{gw}^n = f(1+z)}, \quad (12)$$

where $M_{\text{chirp}} = \mu^{3/5} M^{2/5}$ is the chirp mass of the binary, the total mass M and the reduced mass μ . $f_{gw}^n = n f_{\text{orb}}$ is the eccentric orbit binary emits GWs of harmonics of the orbital frequency with $n \geq 2$, and f is the GW frequency in the observer's frame. While $e = 0$, the above equation reduces to the circular orbit case, since $\Psi(e = 0) = 1$, $g(n = 2, e = 0) = 1$, and $g(n \neq 2, e = 0) = 0$. Here $g(n, e)$ and $\Psi(e)$ are described as follows

$$g(n, e) = \frac{n^4}{32} \left\{ [J_{n-2}(ne) - 2eJ_{n-1}(ne) + \frac{2}{n}J_n(ne) + 2eJ_{n+1}(ne) - J_{n+2}(ne)]^2 + (1 - e^2) [J_{n-2}(ne) - 2J_n(ne) + J_{n+2}(ne)]^2 + \frac{4}{3n^2} [J_n(ne)]^2 \right\}, \quad (13)$$

$$\Psi(e) = \frac{1 + 73/24e^2 + 37/96e^4}{(1 - e^2)^{7/2}}, \quad (14)$$

where J_n are the Bessel functions.

For BBHs, GW radiated in the merger and ring-down phases are also quite important while calculating the SGWB and SNR (e.g., Abbott et al. 2017a). For the merger phase, we assume that the GW energy is confined to the frequency regime of $f > f_i$, where f_i could be taken as (e.g., Kidder, Will, & Wiseman 1993; Lai & Wiseman 1996)

$$f_i \sim \frac{c^3}{6\sqrt{6}GM}. \quad (15)$$

The merger phase will end when the waveform can be described by the $l = m = 2$ quasi-normal mode signal of a Kerr BH. The quasi-normal ringing frequency gives the upper bound of the GW frequency radiated in the merger phase (Flanagan & Hughes 1998)

$$f_q \sim \frac{F(a)c^3}{2\pi GM}, \quad (16)$$

where $F(a) = 1 - 0.63(1 - a)^{3/10}$ and $a = 0.7$ is the dimensionless spin parameter of the BH (e.g., Abbott et al. 2016a,b, 2017a). The total energy radiated in the merger phase is (Kobayashi & Mészáros 2003)

$$E_m = \epsilon_m \left(\frac{4\mu}{M} \right)^2 Mc^2, \quad (17)$$

where $\epsilon_m = 0.05$ is the parametrization of the total energy radiated in the coalescence. Although the energy spectrum of the merger phase may have some features related to the dynamical instabilities (Xing, Centrella, & McMillan 1994; Dimmelleier, Font, & Müller 2002), we assume a simple flat spectrum

$$\frac{dE_m}{df_{gw}} = \frac{E_m}{f_q - f_i} \Big|_{f_{gw} = f(1+z)}. \quad (18)$$

For the ring-down phase, the spectrum peaked at f_q with a

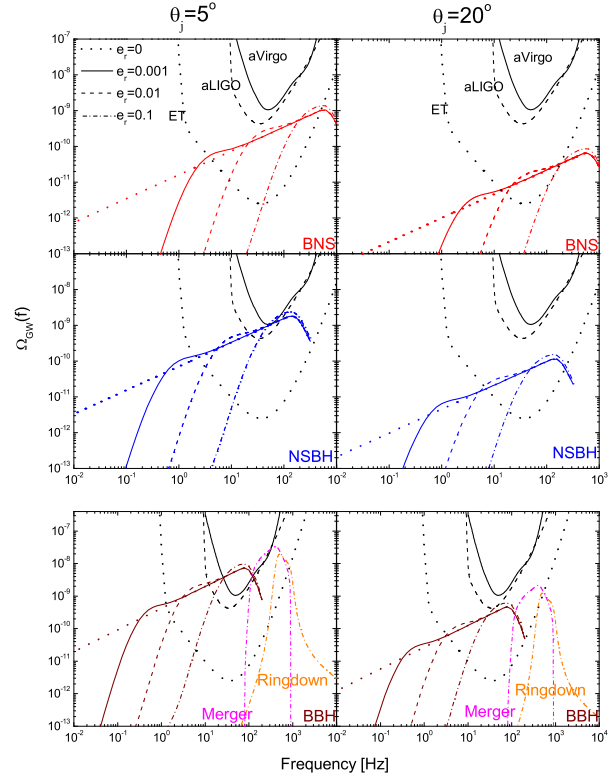


Figure 2. SGWBs from the eccentric BNSs (top panel), NSBH binaries (middle panel), and BBHs (bottom panel). Two jet opening angles of $\theta_j = 5^\circ$ (left) and $\theta_j = 20^\circ$ (right) are considered. The residual eccentricities considered here are: $e_r = 0$ (circular case, dotted lines), $e_r = 0.001$ (solid lines), 0.01 (dashed lines), and 0.1 (dash-dotted lines). For BBHs, SGWBs from the merger (pink dash-dotted line) and ring-down phases (orange dash-dotted line) are also calculated. The detection thresholds of the advanced Virgo (aVirgo), aLIGO, and ET telescopes are shown as black lines for one year of observation.

width of $\Delta f \sim \tau^{-1} = \pi f_q / Q(a)$ with $Q(a) = 2(1 - a)^{-9/20}$ (Echeverria 1989):

$$\frac{dE_r}{df_{gw}} \sim \frac{E_r f^2}{4\pi^4 f_q^2 \tau^3} \times \left\{ \frac{1}{[(f_{gw} - f_q)^2 + (2\pi\tau)^{-2}]^2} + \frac{1}{[(f_{gw} + f_q)^2 + (2\pi\tau)^{-2}]^2} \right\} \Big|_{f_{gw} = f(1+z)} \quad (19)$$

where $E_r = \epsilon_r (4\mu/M)^2 Mc^2$ is the total energy radiated in the ring-down phase. We assume $\epsilon_r = 0.01$ as a nominal parameter (Kobayashi & Mészáros 2003).

SGWB is always described by the dimensionless energy density parameter of $\Omega_{\text{GW}}(f)$, which is the present GW energy density per logarithmic frequency interval divided by the critical energy density of the present universe ($\rho_c c^2$) (Phinney 2001),

$$\Omega_{\text{GW}}(f) = \frac{1}{\rho_c c^2} \frac{d\rho_{\text{gw}}}{d \ln f}, \quad (20)$$

where ρ_{gw} is the GW energy density, f is the frequency in the observer's frame, and $\rho_c = 3H_0^2/8\pi G$ is the critical energy density of the universe. For the astrophysical origin of the GW background, $\Omega_{\text{GW}}(f)$ can be given by

$$\Omega_{\text{GW}}(f) = \frac{f}{\rho_c c^3} F(f), \quad (21)$$

where $F(f)$ is the integrated GW flux at the observed frequency f ,

which can be described by

$$F(f) = \int F_s(f, z) \frac{R_{\text{merger}}(z)}{1+z} dV(z), \quad (22)$$

$F_s(f, z)$ is the observed GW fluence of a single source

$$F_s(f, z) = \frac{(1+z)^2}{4\pi d_L^2} \left. \frac{dE}{df_{\text{gw}}} \right|_{f_{\text{gw}}=f(1+z)}, \quad (23)$$

we use equations (12), (18) and (19) to calculate the SGWBs from the in-spiral, merger and ring-down phases, respectively. Here d_L is the luminosity distance. Combining the binary merger rate derived from SGRBs of equation (10) with equations (11)-(23), we simplify $\Omega_{\text{GW}}(f)$ by

$$\Omega_{\text{GW}}(f) = \int_{z_{\min}}^{z_{\max}} \frac{8\pi G}{3H_0^2 c^2} \frac{R_{\text{merger}}(z)}{(1+z)} \frac{f}{\varepsilon(z)} \left(\frac{dE}{df_{\text{gw}}} \right) \Big|_{f_{\text{gw}}=f(1+z)} dz, \quad (24)$$

here $\varepsilon(z) = \sqrt{\Omega_M(1+z)^3 + \Omega_\Lambda}$. For the in-spiral phase, we set $z_{\min} = 0$ and $z_{\max} = 6$ for $f < f_{\text{max}}/(1+z_{\max})$, otherwise $z_{\max} = f_{\text{max}}/f - 1$ (Rosado 2011; Wu et al. 2012). The maximum frequency $f_{\text{max}} = (1 - e_r^2)^{3/4} c^3 / 6 \sqrt{6} G M$ corresponds to the last stable orbit of the binary, with the semi-minor axis three times the Schwarzschild radius of each star. For the merger and ring-down phases, we set $z_{\min} = 0$ and $z_{\max} = 6$.

The eccentricity evolves as the orbital decay because of the GW radiation. The evolution of the semi-major axis and eccentricity can be described in the quadruple approximation by the differential equations in Peters & Mathews (1963). The eccentricity and semi-major axis evolve according to the two differential equations of

$$\frac{da}{dt} = -\frac{\beta}{a^3} \Psi(e) \quad \beta = \frac{64}{5} \frac{GM_1 M_2 M}{c^5}, \quad (25)$$

$$\frac{de}{dt} = -\frac{19}{12} \frac{\beta}{a^4} \Theta(e) \quad \Theta(e) = \frac{(1 + 121/304 e^2)e}{(1 - e^2)^{5/2}}. \quad (26)$$

Especially, we assume that all binaries do not reach the circular orbit at the last stable orbits ($a_{\min} = 6GM/c^2 \sqrt{1 - e_r^2}$) but with a same residual eccentricity (e_r). For comparison, we give a set values of $e_r = 0.001, 0.01$, and 0.1 . Combining equations (25)-(26) with the final condition of the in-spiral phase ($e_r = 0.001, 0.01$, and 0.1 at a_{\min}), we derive the evolution of the eccentricity (e) with the semi-major axis (a). Here, we do not care about the initial separation of the binary or the initial eccentricity but stopped reversing at $a_0 = 10^{12}$ cm (where $e_0 \approx 1$), because GWs radiated at $a > a_0$ nearly have no contribution to SGWB in and near the detection bands of aLIGO/aVirgo (e.g., $0.1\text{Hz} < f < 1000\text{Hz}$).

We show the SGWBs generated by the eccentric BNSs, NS-BHs, and BBHs with two opening angles of $\theta_j = 5^\circ$ (left panel; the upper limit of SGWBs) and $\theta_j = 20^\circ$ (right panel, the lower limit of SGWBs) in Figure 2. The masses of the NS and BH are assumed to be $1.4M_\odot$ and $10M_\odot$ ³, respectively. All the binaries are assumed to have the same residual eccentricities before merger, e.g., $e_r = 0.001, 0.01$, and 0.1 . For different SGRB progenitors, GW spectra at low frequencies are greatly suppressed. Especially, binaries with high residual eccentricities (e.g., $e_r \gtrsim 0.1$ for BNSs) will radiate GWs in the high frequency bands (e.g., $f > 100\text{Hz}$), which even could be out of the detection bands of aLIGO/aVirgo. It means

³ Theoretically, the masses of the stellar-mass BHs could range from a few solar masses to sever hundred solar masses (Heger & Woosley 2002). However, BH masses measured in X-ray binaries are concentrated in $10 M_\odot$ (e.g., Casares & Jonker 2014), and are mostly $30 M_\odot$ in the observed BBH merger events (Abbott et al. 2016c, 2017a,d).

the non-detection of the SGWB could be resulted by the high residual eccentricities of binaries before merger. We also calculated the SGWBs from NSBHs and BBHs (as shown in the middle and bottom panels of figure 2), both SGWBs are higher than that of BNSs, but the maximum frequencies of the in-spiral phase are lower, because f_{max} is proportional to M^{-1} . The effects of the eccentricity on SGWBs are similar for all SGRB progenitors, e.g., suppressing the SGWB at low frequencies. Especially, SGWBs from BBHs are the strongest, and the merger and ring-down phases also contribute a lot to SGWBs at high frequencies. It is quite expected that SGWBs from the merger of BBHs could be detected by aLIGO/aVirgo in the near future.

The chosen of different SFR models nearly have no effect on SGWBs, which could be clarified if we change equation (24) into

$$\begin{aligned} \Omega_{\text{GW}}(f) &= \langle N \rangle \frac{8\pi G}{3H_0^2 c^2} \frac{(1+z)^2}{4\pi d_L^2} f \left(\frac{dE}{df_{\text{gw}}} \right) \Big|_{f_{\text{gw}}=f(1+z)} \\ &\approx \frac{f}{\rho c^3} F_s(f, z) \langle N \rangle, \end{aligned} \quad (27)$$

where $\langle N \rangle$ is the total SGRB rate, which is only determined by the observed SGRB number. $F_s(f, z)$ is the GW fluence from a single source, which is slightly affected by the redshift. In fact, the redshift effect is negligible, because SGRBs are concentrated in a narrow redshift range of $z \sim 1$.

4 GW-SGRB CO-DETECTION RATE FROM ECCENTRIC ORBIT BINARIES

The co-detection of GWs associate with SGRBs could reduce the search time and increase the detection sensitivity while comparing with the all-sky, all-time search (Bartos & Marka 2015; Clark et al. 2015). The co-detected events are expected to almost face on, and the search time of the GW events could be a few seconds around the burst of SGRBs (Aasi et al. 2014). Therefore, we use the designed sensitivity curve of aLIGO to calculate the detection distance of the GW events (Abbott et al. 2016e) and assume an all sky field of view for SGRB observations.

To determinate whether a GW event is detectable or not, we need to calculate its signal to noise ratio (SNR). For one single event, the SNR could be written as (e.g., Regimbau et al. 2015)

$$\rho^2 = 4 \int_0^\infty \frac{|\tilde{h}_+ F_+ + \tilde{h}_\times F_\times|^2}{S_n(f)} df, \quad (28)$$

where f is the observed GW frequency, \tilde{h}_+ and \tilde{h}_\times are the Fourier transforms of the GW strain amplitudes, F_+ and F_\times are the antenna response functions of the detector (Thorne 1987), and $S_n(f)$ is the one-sided noise power spectral density of aLIGO (e.g., Flanagan & Hughes 1998). Combining equations (12), (18), and (19) in this paper with equation (3) in Regimbau et al. (2015), we could derive the SNR for the eccentric orbit binary mergers

$$\rho^2 = \frac{5}{2} \frac{G(1+z)^2 \mathcal{F}^2}{c^3 \pi^2 d_L^2} \int_{f_{\min}}^{f_{\max}} \frac{f^{-2}}{S_n(f)} \left(\frac{dE}{df_{\text{gw}}} \right) \Big|_{f_{\text{gw}}=f(1+z)} df. \quad (29)$$

The factor

$$\mathcal{F}^2 = \frac{(1 + \cos^2 \iota)^2}{4} F_+^2 + \cos^2 \iota F_\times^2 \quad (30)$$

characterizes the detector response. Here ι is the inclination angle, and only the inclination angle within the SGRB opening angle could be observed as GW-SGRB event. Therefore, we have $\cos \theta_j \leq \cos \iota \approx 1$.

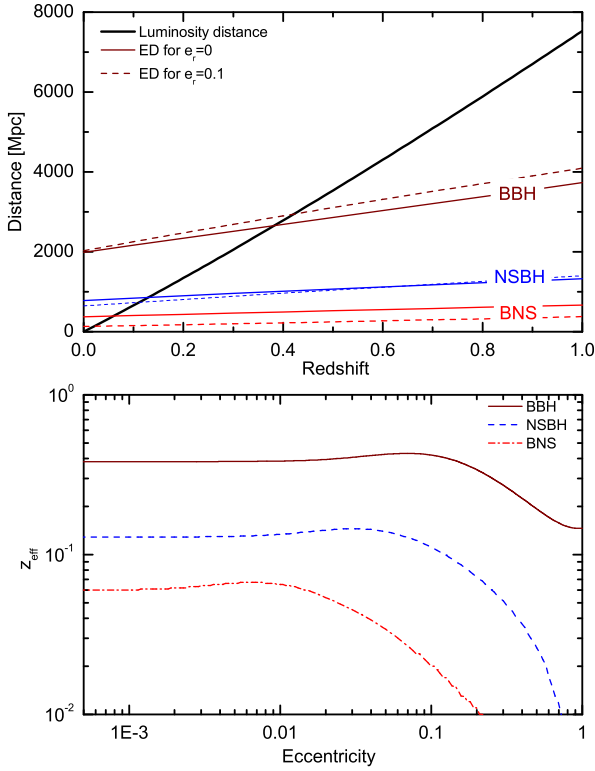


Figure 3. Top: The effective distance (ED) of the GW events (thin lines) and the luminosity distance of SGRBs (thick line). Three SGRB progenitors are considered. The thin solid and dashed lines are for binaries with residual eccentricities of $e_r = 0$ and $e_r = 0.1$, respectively. Bottom: The maximum redshift where SGRB could be detected with GW signal.

To calculate the detectable volume of aLIGO, we need to know the detectable distance of the source, here we adopted the so-called effective distance (ED), which is related to d_L through $D_{\text{eff}} = d_L / \mathcal{F}$ (Allen et al. 2012). When averaging F_+ and F_\times over the uniformly distributed θ (the right ascension of the source), ϕ (the declination of the source) and ψ (the polarization angle), we obtain $\langle F_+^2 \rangle = \langle F_\times^2 \rangle = \sin^2 \zeta / 5$, where $\zeta = 90^\circ$ is the opening angle between two arms of aLIGO. Therefore, the detectable distance could be written as

$$D_{\text{eff}} = \frac{1+z}{\rho} \left(\frac{5G}{2\pi^2 c^3} \right)^{1/2} \sqrt{\int_{f_{\min}}^{f_{\max}} \frac{f^{-2}}{S_n(f)} \left(\frac{dE}{df_{\text{gw}}} \right) \bigg|_{f_{\text{gw}}=f(1+z)} df}. \quad (31)$$

In our calculation, the threshold SNR is set to be $\rho = 8$ (Abbott et al. 2016e). Specially, we should note that only GWs from the in-spiral phase are used to calculate the SNR for BNS and NS-BHs, because GWs from the merger and ring-down phases are out of the sensitive band of aLIGO/aVirgo. For BBHs, three phases are considered to calculate the SNR.

Only SGRBs within the detectable distance of aLIGO could be observed as the GW-SGRB events, therefore, ED should be greater than the luminosity distance. As shown in the top panel of figure 3, only SGRBs with redshifts smaller than the cross point of ED and d_L could be observed as the GW-SGRB events. We found that ED is slightly dependent on the redshift for low mass binaries (e.g., BNSs and NSBHs), but more dependent for high mass binaries like BBHs. To study the effect of the eccentricity on GW-SGRB co-detection rate, we calculated the maximum redshift-eccentricity re-

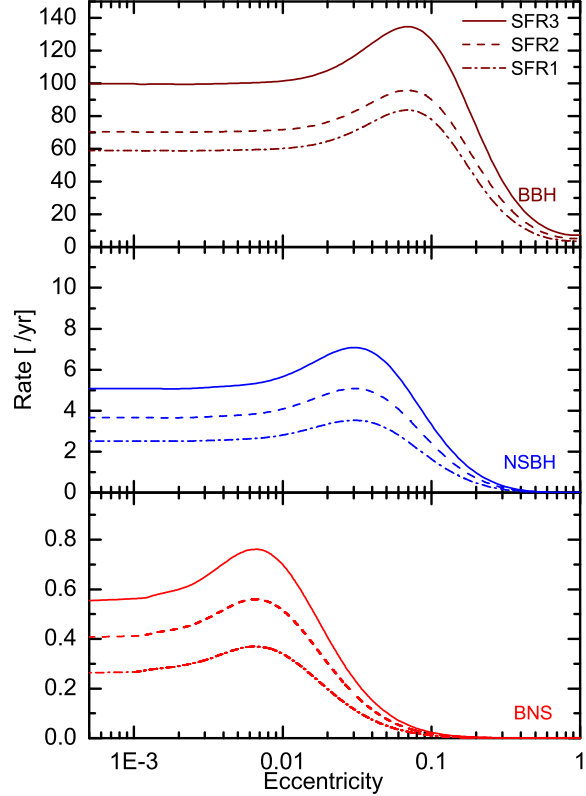


Figure 4. The co-detection rate of GW-SGRB event versus the residual eccentricity. Three types of SGRB progenitors are considered: BBHs (wine lines), NSBH binaries (blue lines), and BNSs (red lines). The dash-dotted (SFR1), dashed (SFR2), and solid lines (SFR3) represent three SFR models used in the paper.

lations for different binary systems, which are shown in the bottom panel of figure 3.

Finally, the GW-SGRB co-detection rate is a function of the observed SGRB rate $R_{\text{SGRB}}(z)$ and the detectable volume of the GW event, which can be described by

$$R_{\text{co}}(e_r) = \int_0^{\infty(e_r)} \frac{R_{\text{SGRB}}(z)}{(1+z)} dV(z), \quad (32)$$

where $R_{\text{SGRB}}(z)$ is the observed SGRB rate derived in section 2, $dV(z)$ is the detectable volume of the GW event. In figure 4, we show the GW-SGRB co-detection rates as a function of the residual eccentricity. Three cases such as BNSs (red lines), NSBHs (blue lines) and BBHs (wine lines) are considered. We found that the GW-SGRB co-detection rates are greatly reduced for binaries with high residual eccentricities ($e_r \gtrsim 0.2$) while comparing with the circular case. Therefore, much more time will be needed for the observation of these events. For example, it will cost 2.6 years (for SFR3) to observe one event for BNSs with $e_r = 0.02$, but 1.8 years (for SFR3) for the circular case. Interestingly, the GW-SGRB co-detection rates could be ~ 1.4 times higher than the circular case within some particular ranges of e_r (shown as the bumps in the figure), depending on the masses of the binaries, e.g., $0.0013 < e_r < 0.014$ for BNSs, $0.002 < e_r < 0.066$ for NSBHs, and $0.005 < e_r < 0.15$ for BBHs. The reason is that more GW energy is contributed from the low-frequency orbits into the frequency band of aLIGO. Furthermore, our results show that the GW-SGRB co-detection rate is nearly ~ 100 per year for BBHs (which could be ~ 32 times higher for $30M_\odot$ of the black hole mass), which

is much higher than the recent observations of the BBH merger rate (4.8/year for the first observing run of the aLIGO, 4.5/year for the second observing run). Therefore, even if all the observed BBHs are SGRB progenitors (let alone only two BBHs may be possible SGRB progenitors), only a small fraction of BBHs could be SGRB progenitors, unless they have very large residual eccentricities before merger (e.g., $e_r > 0.7$ with BBH merger rate of ~ 4 /year). Recent observation of GW170817 confirmed the coalescing model for SGRBs, and the GW-GRB co-detection rate is about 1.5 per year (one event observed in 8 months for the second run of aLIGO), which may implies that not all SGRBs are originated from the mergers of BNSs (0.8 event per year at most), a fraction of BHNSs and BBHs may also be their origin (as shown in figure 4).

5 CONCLUSION AND DISCUSSION

Firstly, we derived the SGRB rate from the *Swift* observations, and the local SGRB rate is consistent with the previous works for different SFR models (Guetta et al. 2009; Siellez et al. 2014; Clark et al. 2015; Wanderman & Piran 2015). Our results show that a constant time delay distribution between the SGRB rate and SFR is preferred. The power law time delay distribution is disfavored by the observations, because it predicts too much dim SGRBs at high-redshifts. However, we stress that the narrow constant time delay distribution could be resulted from the lack of high-redshift SGRBs (e.g., $z > 1.5$). More high-redshift bursts is sufficient to make a difference.

Secondly, we studied the effect of eccentricity on SGWBs for different types of SGRB progenitors, such as BNSs, NSBHs, and BBHs. We found that SGWBs are greatly suppressed at low frequencies (e.g., $f \lesssim 1$ Hz) for eccentric orbit binaries. Particularly, SGWBs from binaries with high residual eccentricities (e.g., $e_r \gtrsim 0.1$ for BNSs) are hard to be detected, because the radiated GW frequencies are above the detection frequency of aLIGO/aVirgo. The chosen of different SFR models have little effect on SGWBs, because the total SGRB number is only determined by the observation. Anyway, it is possible that SGWB from BBHs could be detected by aLIGO for one year of observation. Moreover, SGWB is severely dependent on the merger rate of SGRB progenitors and the black hole mass. For one point, the merger rate could be 16 times lower for $\theta_j = 20^\circ$ while comparing with $\theta_j = 5^\circ$ (e.g., Chen & Holz 2013), therefore, the SGWB could be 16 times weaker, as shown in the right panel of figure 2. For another point, the SGWB could be ~ 6.2 times higher if BBH mass is assumed to be $30 M_\odot$.

Finally, we calculated the GW-GRB co-detection rates. On one hand, we found that the co-detection rates are greatly reduced for binaries with high residual eccentricities (e.g., $e_r \gtrsim 0.2$). And we suggested that the extremely low GW-GRB events may be caused by the high residual eccentricities of binaries before merger. On the other hand, the co-detection rates could be 1.4 times higher than the circular case for binaries with residual eccentricities within some particular ranges, shown as the bumps in figure 4. Additionally, we have observed two possible and one confirmed GW-GRB events: GW150914 (Abbott et al. 2016a; Connaughton et al. 2016; Savchenko et al. 2016), GW170104 (Verrecchia et al. 2017), and GW170817. The average event rate is 2.8 per year (three events in 13 months of the first and second run of aLIGO). Comparing with our results in figure 4, it may implies that not all SGRBs are originated from the mergers of BNSs, mergers of BHNSs and BBHs

may also be their origin. However, based on the recent observations of BBH merger events and the GW-GRB co-detection events, our prediction of ~ 100 GW-GRB events per year (32 times higher for $30 M_\odot$ of the BH mass) from BBH merger seems too high. This means that only a small fraction of BBHs could be SGRB progenitors, unless they have very large residual eccentricities before merger (e.g., $e_r > 0.7$ with BBH merger rate of ~ 4 /year). Specially, we should note that the effect of the eccentricity on the co-detection rate is severely dependent on the sensitivity of the GW detectors. The higher the sensitivity of the GW detectors are, the more low eccentric orbit binaries will be observed, and the plateau in figure 4 will be shorten.

ACKNOWLEDGEMENTS

We thank the anonymous referee for detailed comments and suggestions. This work is supported by the National Basic Research Program of China (973 Program, grant No. 2014CB845800) and the National Natural Science Foundation of China (grants 11422325, 11373022, 11633001 and 11673008), the Excellent Youth Foundation of Jiangsu Province (BK20140016), Jiangsu Planned Projects for Postdoctoral Research Funds (0201003406).

REFERENCES

- Aasi J., et al., 2014, PhRvL, 113, 011102
- Aasi J., et al., 2015, CQGra, 32, 115012
- Abadie J., et al., 2010, CQGra, 27, 173001
- Abbott B., et al., 2008, ApJ, 681, 1419
- Abbott B. P., et al., 2009, PhRvD, 79, 122001
- Abbott B. P., et al., 2016a, PhRvL, 116, 061102
- Abbott B. P., et al., 2016b, PhRvL, 116, 241103
- Abbott B. P., et al., 2016c, ApJ, 832, L21
- Abbott B. P., et al., 2016d, PhRvX, 6, 041015
- Abbott B. P., et al., 2016e, LRR, 19, 1
- Abbott B. P., et al., 2017a, PhRvL, 118, 221101
- Abbott B. P., et al., 2017b, PhRvL, 119, 161101
- Abbott B. P., et al. (LIGO Scientific Collaboration and Virgo Collaboration), 2017c, Astrophys. J. Lett. 848, L13
- Abbott B. P., et al., 2017d, PhRvL, 119, 141101
- Abbott B. P., et al., 2017e, arXiv e-prints, arXiv: 1711.05578v1
- Acernese F., et al., 2008, CQGra, 25, 184001
- Acernese F., et al., 2015, JPhCS, 610, 012014
- Adriani O., et al., 2016, ApJ, 829, L20
- Allen B., Anderson W. G., Brady P. R., Brown D. A., Creighton J. D. E., 2012, PhRvD, 85, 122006
- Anderson S. B., Gorham P. W., Kulkarni S. R., Prince T. A., Wołoszczan A., 1990, Natur, 346, 42
- Ando S., 2004, JCAP, 6, 007
- Antonini F., Perets H. B., 2012, ApJ, 757, 27
- Arcavi I., et al., 2017, ApJ, 848, L33
- Band D., et al., 1993, ApJ, 413, 281
- Bartos I., Brady P., Márka S., 2013, CQGra, 30, 123001
- Bartos I., Marka S., 2015, PhRvL, 115, 231101
- Berger E., 2014, ARA&A, 52, 43
- Bhattacharya D., van den Heuvel E. P. J., 1991, PhR, 203, 1
- Bloom J. S., Sigurdsson S., Pols O. R., 1999, MNRAS, 305, 763
- Bloom J. S., et al., 2006, ApJ, 638, 354
- Brown D. A., Zimmerman P. J., 2010, PhRvD, 81, 024007
- Casares J., Jonker P. G., 2014, SSRv, 183, 223

- Chen H.-Y., Holz D. E., 2013, *PhRvL*, 111, 181101
- Clark J., Evans H., Fairhurst S., Harry I. W., Macdonald E., Macleod D., Sutton P. J., Williamson A. R., 2015, *ApJ*, 809, 53
- Champion D. J., et al., 2008, *Sci*, 320, 1309
- Connaughton V., et al., 2016, *ApJL*, 826, L6
- Connaughton V., et al., 2017, *GCN* 21506, 1
- Coughlin M., Meyers P., Thrane E., Luo J., Christensen N., 2015, *PhRvD*, 91, 063004
- Cowperthwaite P. S., et al., 2016, *ApJ*, 826, L29
- Dewi J. D. M., Podsiadlowski P., Pols O. R., 2005, *MNRAS*, 363, L71
- Dietz A., 2011, *A&A*, 529, A97
- Dimmelmeier H., Font J. A., Müller E., 2002, *A&A*, 393, 523
- East W. E., Pretorius F., 2012, *ApJ*, 760, L4
- East W. E., McWilliams S. T., Levin J., Pretorius F., 2013, *PhRvD*, 87, 043004
- Echeverria F., 1989, *PhRvD*, 40, 3194
- Eichler D., Livio M., Piran T., Schramm D. N., 1989, *Natur*, 340, 126
- Enoki M., Nagashima M., 2007, *PTPh*, 117, 241
- Evangelista E. F. D., de Araujo J. C. N., 2015, *MNRAS*, 449, 2700
- Fong W., et al., 2014, *ApJ*, 780, 118
- Fardal M. A., Katz N., Weinberg D. H., Davé R., 2007, *MNRAS*, 379, 985
- Fermi-GBM O. b. o. t., Fermi-LAT collaborations, 2017, *ArXiv e-prints*, arXiv:1706.00199
- Flanagan É. É., Hughes S. A., 1998, *PhRvD*, 57, 4535
- Gendre B., Barret D., Webb N., 2003, *A&A*, 403, L11
- Gold R., Bernuzzi S., Thierfelder M., Brüggmann B., Pretorius F., 2012, *PhRvD*, 86, 121501
- Goldstein A., et al., 2017a, *GCN* 21528, 1
- Goldstein A., et al., 2017b, *Astrophys. J. Lett.* 848, L14
- Guetta D., Piran T., 2006, *A&A*, 453, 823
- Guetta D., Stella L., 2009, *A&A*, 498, 329
- Grindlay J., Portegies Zwart S., McMillan S., 2006, *NatPh*, 2, 116
- Hao J.-M., Yuan Y.-F., 2013, *A&A*, 558, A22
- Heger A., Woosley S. E., 2002, *ApJ*, 567, 532
- Heinke C. O., Grindlay J. E., Lugger P. M., Cohn H. N., Edmonds P. D., Lloyd D. A., Cool A. M., 2003, *ApJ*, 598, 501
- Howell E. J., Coward D. M., Stratta G., Gendre B., Zhou H., 2014, *MNRAS*, 444, 15
- Huerta E. A., Brown D. A., 2013, *PhRvD*, 87, 127501
- Hulse R. A., Taylor J. H., 1975, *ApJ*, 195, L51
- Ignatiev V. B., Kuranov A. G., Postnov K. A., Prokhorov M. E., 2001, *MNRAS*, 327, 531
- Kalogera V., Narayan R., Spergel D. N., Taylor J. H., 2001, *ApJ*, 556, 340
- Kidder L. E., Will C. M., Wiseman A. G., 1993, *PhRvD*, 47, 3281
- Kobayashi S., Mészáros P., 2003, *ApJ*, 589, 861
- Kopač D., et al., 2012, *MNRAS*, 424, 2392
- Kouveliotou C., Meegan C. A., Fishman G. J., Bhat N. P., Briggs M. S., Koshut T. M., Paciesas W. S., Pendleton G. N., 1993, *ApJ*, 413, L101
- Kowalska I., Bulik T., Belczynski K., 2012, *A&A*, 541, A120
- Lai D., Wiseman A. G., 1996, *PhRvD*, 54, 3958
- Lee W. H., Ramirez-Ruiz E., van de Ven G., 2010, *ApJ*, 720, 953
- Lien A., Sakamoto T., Gehrels N., Palmer D. M., Barthelmy S. D., Graziani C., Cannizzo J. K., 2014, *ApJ*, 783, 24
- Loeb A., 2016, *ApJ*, 819, L21
- Mandel I., 2016, *MNRAS*, 456, 578
- Mészáros P., Rees M. J., 1992, *MNRAS*, 257, 29P
- Narayan R., Paczynski B., Piran T., 1992, *ApJ*, 395, L83
- O’Leary R. M., Kocsis B., Loeb A., 2009, *MNRAS*, 395, 2127
- Osłowski S., Bulik T., Gondek-Rosińska D., Belczyński K., 2011, *MNRAS*, 413, 461
- Paczynski B., 1986, *ApJ*, 308, L43
- Paczynski B., 1991, *AcA*, 41, 257
- Peters P. C., Mathews J., 1963, *PhRv*, 131, 435
- Phinney E. S., 2001, *astro*, arXiv:astro-ph/0108028
- Pooley D., et al., 2003, *ApJ*, 591, L131
- Portegies Zwart S. F., Yungelson L. R., 1998, *A&A*, 332, 173
- Regimbau T., Mandic V., 2008, *CQGra*, 25, 184018
- Regimbau T., Siellez K., Meacher D., Gendre B., Boër M., 2015, *ApJ*, 799, 69
- Robertson B. E., Ellis R. S., 2012, *ApJ*, 744, 95
- Rosado P. A., 2011, *PhRvD*, 84, 084004
- Samsing J., MacLeod M., Ramirez-Ruiz E., 2014, *ApJ*, 784, 71
- Sari R., Piran T., Halpern J. P., 1999, *ApJ*, 519, L17
- Savchenko V., et al., 2016, *ApJ*, 820, L36
- Savchenko V., et al., 2017a, *ApJ*, 846, L23
- Savchenko V., et al., 2017b, *GCN* 21507, 1
- Savchenko V., et al., 2017c, *Astrophys. J. Lett.* 848, L15
- Siellez K., Boër, and Gendre B., 2014, *MNRAS* 437, 649
- Springel V., Hernquist L., 2003, *MNRAS*, 339, 312
- Stephens B. C., East W. E., Pretorius F., 2011, *ApJ*, 737, L5
- Tan W.-W., Wang F. Y., 2015, *MNRAS*, 454, 1785
- Tanvir N. R., Levan A. J., Fruchter A. S., Hjorth J., Hounsell R. A., Wiersema K., Tunnicliffe R. L., 2013, *Natur*, 500, 547
- Thompson T. A., 2011, *ApJ*, 741, 82
- Thorne K. S., in *300 Years of Gravitation*, edited by Hawking S.W. and Israel W. (Cambridge University Press, Cambridge, England, 1987), pp. 330-458
- Tsutsui R., Yonetoku D., Nakamura T., Takahashi K., Morihara Y., 2013, *MNRAS*, 431, 1398
- Tumlinson J., Shull J. M., 2000, *ApJ*, 528, L65
- Verrecchia F., et al., 2017, *ApJ*, 847, L20
- von Kienlin A. G. A., Meegan C., and the Fermi GBM Team, 20017, *GCN* 21520, 1
- Wanderman D., Piran T., 2015, *MNRAS*, 448, 3026
- Wang F. Y., 2013, *A&A*, 556, A90
- Williamson A. R., Biwer C., Fairhurst S., Harry I. W., Macdonald E., Macleod D., Predoi V., 2014, *PhRvD*, 90, 122004
- Wu C., Mandic V., Regimbau T., 2012, *PhRvD*, 85, 104024
- Xing Z., Centrella J. M., McMillan S. L. W., 1994, *PhRvD*, 50, 6247
- Zhang B., 2016, *ApJL*, 827, L31
- Zhang, G. Q., Wang, F. Y., arXiv: 1711.08206
- Zhu X.-J., Howell E. J., Blair D. G., Zhu Z.-H., 2013, *MNRAS*, 431, 882